A-, T-, and H-type Currents Shape Intrinsic Firing of Developing Rat Abducens Motoneurons

Michaël Russier, Edmond Carlier, Norbert Ankri, Laure Fronzaroli, Dominique Debanne

A-, T-, and H-type currents shape intrinsic firing of developing rat abducens motoneurons

Michaël Russier, Edmond Carlier, Norbert Ankri, Laure Fronzaroli and Dominique Debanne

Neurobiologie des Canaux Ioniques, INSERM U464, IFR Jean Roche, Faculté de Médecine Nord, Université de la Méditerranée, Boulevard Pierre Dramard, 13916 Marseille Cedex 20, France

During postnatal development, profound changes take place in the excitability of nerve cells, including modification in the distribution and properties of receptor-operated channels and changes in the density and nature of voltage-gated channels. We studied here the firing properties of abducens motoneurons (aMns) in transverse brainstem slices from postnatal day (P) 1–13 rats. Recordings were made from aMNs in the whole-cell configuration of the patch-clamp technique. Two main types of aMn could be distinguished according to their firing profile during prolonged depolarizations. Both types were identified as aMns by their fluorescence following retrograde labelling with the lipophilic carbocyanine DiI in the rectus lateralis muscle. The first type (BaMns) exhibited a burst of action potentials (APs) followed by an adaptation of discharge and were encountered in ~70 % of aMns. Their discharge profile resembled that of adult aMns and was encountered in all aMns after P9. BaMns exhibited a hyperpolarization-induced rebound potential that was blocked by low concentrations of Ni^{2+} or by Ca^{2+}-free external solution. This current had the properties of the T-type current. Action potentials of BaMns showed a complex afterhyperpolarization (AHP). An inward rectification was evidenced following hyperpolarization and was blocked by external application of caesium or ZD7288, indicating the presence of the hyperpolarization-activated cationic current (I_H). Blocking the I_H current almost doubled the input resistance of BaMns. The second class of aMns (DaMns) displayed a delayed excitation that was mediated by A-type K^+ currents and was observed only between P4 and P9. DaMns exhibited immature characteristics: an action potential with a simple AHP, a linear current–voltage relation and a large input resistance. The number of aMns remained unchanged when both types were present (P5–P6) and later in development when only BaMns were encountered (P19), suggesting that DaMns mature into BaMns during postnatal development. We conclude that aMns display profound reorganization in their intrinsic excitability during postnatal development.

Corresponding authors D. Debanne: Neurobiologie des Canaux Ioniques, INSERM U464, IFR Jean Roche, Faculté de Médecine Nord, Université de la Méditerranée, Boulevard Pierre Dramard, 13916 Marseille Cedex 20, France. Email: debanne.d@jean-roche.univ-mrs.fr

The rat abducens nucleus is a small brainstem nucleus containing approximatively 150–330 motoneurons that innervate the rectus lateralis muscle (Cabrera *et al.* 1988). Abducens motoneurons (aMns) ensure a fast, horizontal rotation of the ocular globe during saccades and allow the stabilization of gaze in a given horizontal position during fixation (Robinson, 1981; Godaux & Chéron, 1993). During a saccade, aMns exhibit a phasic burst of action potentials (APs) followed by a tonic discharge (Delgado-Garcia *et al.* 1986*b*). This profile of neuronal discharge is thought to be particularly well adapted to compensate the inertia of the ocular globe for initiating the gaze movement (Robinson, 1981). During ocular fixation, the firing rate of aMns remains constant and relatively precise (Gómez *et al.* 1986). In the adult rat *in vivo*, aMns exhibit also an initial burst of APs in response to long depolarizing pulses of current (Durand, 1989). In contrast to other well-studied brainstem motoneurons (review in Rekling *et al.* 2000), intrinsic currents have never been characterized in aMns, because an *in vitro* preparation to study these neurons was lacking. The knowledge of the firing properties of aMns comes from several intracellular studies in the adult cat and rat *in vivo* (Baker & Highstein, 1975; Grantyn & Grantyn, 1978; Durand, 1989).

We took advantage of the recent development of an *in vitro* preparation of identified aMns (Russier *et al.* 2002) to study the discharge pattern and the underlying voltage-gated conductances in rat aMns during the first 2 weeks of postnatal development. Unexpectedly, we observed a striking functional heterogeneity of aMns during development. The main functional type of aMn corresponds to the adult type and exhibits an initial bursting discharge profile (BaMns) due to the presence of prominent T-type Ca^{2+} and H-type cationic currents. The

second type of aMn exhibits a delayed firing profile (DaMn) and is transiently observed between P4 and P9. The delayed firing of these neurons results mainly from the expression of a powerful 4-aminopyridine (AP)-sensitive, A-type K^+ current. However, some specific features of BaMns such as the I_H current or the complex afterhyperpolarization (AHP) of the action potential were also encountered in DaMns. In addition, the number of aMns remained constant, but the distribution changed from half DaMns and half BaMns to all BaMns. We conclude that the relative proportion of these three conductances determines the functional profile of aMns indicating that these two types are not mutually exclusive but rather form a continuum from which each type represents the extremes.

METHODS

Retrograde labelling of abducens motoneurons

One day before the experiment, 1- to 13-day-old Wistar rats were deeply anaesthetized with chloral hydrate (I.P., 200 mg kg^{-1}). All experiments were carried out according to European and national guidelines for the care and use of laboratory animals (Council Directive 86/609/EEC and French National Research Council). A solution of carbocyanin at 15 % in ethanol (*FAST* DiI, Molecular Probes) was injected behind the eye, close to the rectus lateralis muscle (Russier *et al.* 2002). Animals were regularly monitored during recovery from their initial anaesthesia in a temperature- and humidity-controlled box. The day after the injection, animals were deeply anaesthetized and killed by decapitation.

Slice preparation

Transverse brainstem slices (300 μm thick) containing the abducens nucleus were prepared with a vibroslicer (Leica VT-1000S). The slicing solution, maintained at 4 °C, contained (mM): 280 sucrose, 26 $NaHCO_3$, 10 D-glucose, 1.3 KCl, 1 $CaCl_2$ and 10 $MgCl_2$. The abducens nucleus was localized using fluorescent microscopy at low magnification (×4 or ×10). Abducens motoneurons were then identified at higher magnification (×40) by their fluorescent staining, and visualized with an infrared video-microscopy device. All experiments were performed in a temperature-controlled (34 °C) submerged slice chamber (Luigs and Neumann, Ratingen, Germany).

Electrophysiology

Whole-cell patch-clamp recordings were obtained from identified aMns with an Axoclamp-2B amplifier (Axon Instruments) in bridge mode or in single electrode voltage-clamp in the continuous mode. Some experiments were performed with an Axopatch-200B amplifier (Axon Instruments). Membrane potentials or currents were filtered (3–5 kHz low-pass). Digitized signals (18 kHz, Instrutech VR-100B) were stored on videotape for later analysis via the Digidata interface (Axon Instruments; sampling rate 10–12 kHz) with the use of Acquis1 software (Gérard Sadoc, Biologic/Unité de Neurosciences Integratives et Computationelles (UNIC), CNRS, France). In some experiments, voltage-gated currents were characterized with the use of pCLAMP6 (Axon Instruments; sampling rate 8–10 kHz). The extracellular saline was defined in Russier *et al.* (2002) and contained (mM): 125 NaCl, 2.5 KCl, 1.1 NaH_2PO_4, 26 $NaHCO_3$, 4 $CaCl_2$ and 0.5 $MgCl_2$. The relatively high Ca^{2+}/Mg^{2+} ratio had no incidence on the firing properties. When this ratio was decreased from 4/0.5 to 3/2, the firing remained virtually unchanged ($n = 3$ aMns). Internal solution for filling the patch pipette contained (mM): 20 KCl, 120 potassium gluconate, 10 Hepes, 10 EGTA, 2 $MgCl_2$, 2 Na_2ATP (pH 7.4). EGTA has no influence on the mAHP of pyramidal neurons (Storm, 1987). Abducens motoneurons were recorded with a pipette containing 0.5 mM EGTA ($n = 3$ cells). In these conditions, the mAHP was virtually identical to that described in neurons recorded with 10 mM EGTA. For the characterization of voltage-gated calcium currents, the internal solution for filling the patch pipette contained (mM): 140 CsCl, 5 Hepes, 2 $MgCl_2$, 2 NaATP (pH 7.4). Neurons were voltage-clamped at −80 mV. Series resistance was in the range of 15–30 MΩ and ~20 % series compensation was routinely used. ZD7288 was obtained from Tocris Cookson. Mibefradil was a gift from Dr Nargeot (CNRS, Montpellier, France). All other drugs were from Sigma.

Data analysis

Postsynaptic currents and potentials were analysed with the help of Acquis1 (Gérard Sadoc, UNIC, CNRS Gif-sur-Yvette, France) and Detectivent (Norbert Ankri, INSERM U464 Marseille, France). The rate of firing accommodation was expressed by calculating the ratio (r) of the first interspike interval (a) to that of the third interspike interval (b) (Fig. 2*A*). These measurements were made at a holding membrane potential more negative than −70 mV (range −80 to −70 mV) and for a mean spike frequency of ~10 Hz. The ratio (r) was less than 1 for accommodating neurons with an initial burst (BaMns) and greater than 1 for accelerating neurons that exhibited a delayed excitation (DaMns).

Immunohistochemistry

Four rats were used to compare the number of choline acetyl transferase (ChAT) immunopositive aMns at P5–P6 (2 rats) and P19–P20 (2 rats). After deep anaesthesia, animals were killed by decapitation and the brainstem was removed. A block containing the abducens nuclei was cut out and immersed for 72 h in a fixative solution containing 4 % paraformaldehyde in 0.1 M phosphate buffer (pH 7.4). The block was serially cut in 40 μm sections with a vibro-slicer (Leica VT-1000S) and kept in the same fixative solution for 48 h. The sections were incubated with a goat anti-ChAT primary antibody (24 h at room temperature, 1 : 2000, Chemicon). The primary antibody was revealed by a biotinylated goat anti-rabbit secondary antibody (2 h at room temperature, 1 : 200, Vector). The biotinylated antibody was then reacted with avidin–biotin complex coupled to HRP and revealed with di-amino benzidine (Vector). The sections were mounted on gelatin-coated slides, air dried, dehydrated through series of graded ethanol solutions and mounted in Eukitt medium. Each section was digitized with a video-microscopy device (camera: Donpisha XC-003P; microscope: Nikon eclipse TE300) and neurons were counted on each section and summed for each abducens nucleus.

Identification of recorded aMns

aMns (127 in total) were recorded in the whole-cell configuration of the patch-clamp technique in stable conditions. During subsequent analysis, this sample was reduced to 109 aMns. Eighty-six motoneurons were studied for their firing properties in current clamp whereas 23 aMns were studied for their voltage-gated currents in voltage-clamp conditions. Nineteen recorded neurons were identified by their fluorescence after retrograde labelling with DiI (Plant *et al.* 1998; Russier *et al.* 2002). Among this sample, 15 neurons were also identified for their electrophysiological properties in current clamp. The rest of the sampled neurons were not labelled. In this case, specific care was taken to record neurons

Table 1. Electrophysiological characteristics of BaMns and DaMns recorded in brainstem slices from P4–P9 rats

Type	n	R_{in} (MΩ)	AP amplitude (mV)	AP half-width (ms)	Soma length (μm)	V_m (mV)
BaMns	33	323 ± 49	63 ± 1	1.41 ± 0.11	21.3 ± 0.7 (n = 3)	−56.4 ± 1.7
DaMns	23	591 ± 66	65 ± 3	1.60 ± 0.10	24.9 ± 0.7 (n = 3)	−59.4 ± 2.0
Mann-Whitney		$P < 0.01$	n.s.	n.s.	n.s.	n.s.

R_{in}, input resistance; V_m, resting membrane potential.

Table 2. Development of electrophysiological properties of BaMns

Age	n	R_{in} (MΩ)	AP amplitude (mV)	AP half-width (ms)	T-type rebound
P2–P3	6	829 ± 161*	58 ± 4*	1.64 ± 0.24†	4/6
P4–P5	8	568 ± 143	64 ± 4	1.49 ± 0.2	7/8
P6–P7	11	281 ± 62	63 ± 2	1.66 ± 0.2	8/9
P8–P9	14	216 ± 40	63 ± 2	1.27 ± 0.16	7/7
P10–P13	6	372 ± 37*	69 ± 4*	1.27 ± 0.17†	5/5

Comparison between P2–P3 and P10–P13 BaMns, *Mann-Whitney, $P < 0.05$, † n.s.

that were putative abducens motoneurons, i.e. neurons with large somata (> 20 μm), mostly located in the medial part of the nucleus (Cabrera *et al.* 1988). Preliminary physiological classification on the basis of spiking pattern was determined during the first 2–5 min following establishment of the whole-cell recording configuration. However, more detailed investigation required longer recordings and cells were tested multiple times throughout the experiments to control for possible instability or washout of calcium current. No changes in the firing pattern were observed over the course of the recording.

RESULTS

Overview of distinguishing features

Two main types of aMn were characterized by their firing profile during prolonged depolarizations. The first type of aMn (BaMns) exhibited an initial burst of APs at high frequency (up to 50–200 Hz) followed by a slight adaptation (Fig. 1*A*). These characteristics were usually better seen when the neuron was hyperpolarized below −70 mV. In contrast, the second type (DaMns) exhibited a delayed excitation and a progressive acceleration of the instantaneous firing frequency (Fig. 1*B*). Both types could be identified as retrogradely labelled neurons within the abducens nucleus (6 BaMns and 9 DaMns, see inset in Fig. 1*A* and *B*) and therefore correspond to aMns.

We have systematically studied the firing pattern of 70 aMns by measuring an index of instantaneous firing adaptation (r) when the neurons were held at a hyperpolarized membrane potential (< −70 mV; see Methods and Fig. 2*A*). The distribution of the index was continuous (Fig. 2*B*), but abducens motoneurons were arbitrarily divided into two main classes: neurons exhibiting an increase in the instantaneous discharge frequency ($r > 1$, DaMns) and those showing a decrease in the instantaneous firing frequency ($r < 1$, BaMns).

Abducens motoneurons with a bursting discharge (BaMns)

BaMns exhibited several characteristics of mature motoneurons. They had an action potential with a complex AHP. The first phase of the AHP peaks early and corresponds to the fast AHP (fAHP, Storm, 1990; Viana *et al.* 1993*a,b*). This component contributes to the repolarization of the AP (Fig. 3*A*). The second phase peaks later, 20–50 ms after the AP, and has a more prolonged time course. This component corresponds to the medium AHP (mAHP, Storm, 1990; Viana *et al.* 1993*b*). These two phases were separated by a depolarizing waveform, the afterdepolarization (ADP). This ADP has been quantified systematically by measuring the amplitude of the positive component on the derivative of the first AP. This amplitude was negatively correlated with the index of firing accommodation (Fig. 3*C*), indicating that BaMns but not DaMns express a complex AHP.

BaMns represented 70 % of the total population (47/70) and were encountered at all postnatal ages, but they made up the total population of recorded neurons in rats older than P9 (n = 8 cells, Fig. 2*C* and *D*). Between P4 and P9, BaMns had a relatively low input resistance (323 ± 49 MΩ, n = 33). The mean accommodation index of BaMns was 0.65 ± 0.04 (n = 45). The general characteristics of BaMns between P4 and P9 are summarized in Table 1. The development profile of the electrophysiological properties of BaMns shows a significant decrease in input resistance and an increase in the spike amplitude (Table 2), as previously observed in other developing brainstem neurons (Viana *et al.* 1994; Murphy & Du Lac, 2001).

Abducens motoneurons with a delayed firing (DaMns)

DaMns represented nearly 30 % of the total population of aMns between P2 and P13 (23/70). For all DaMns, the

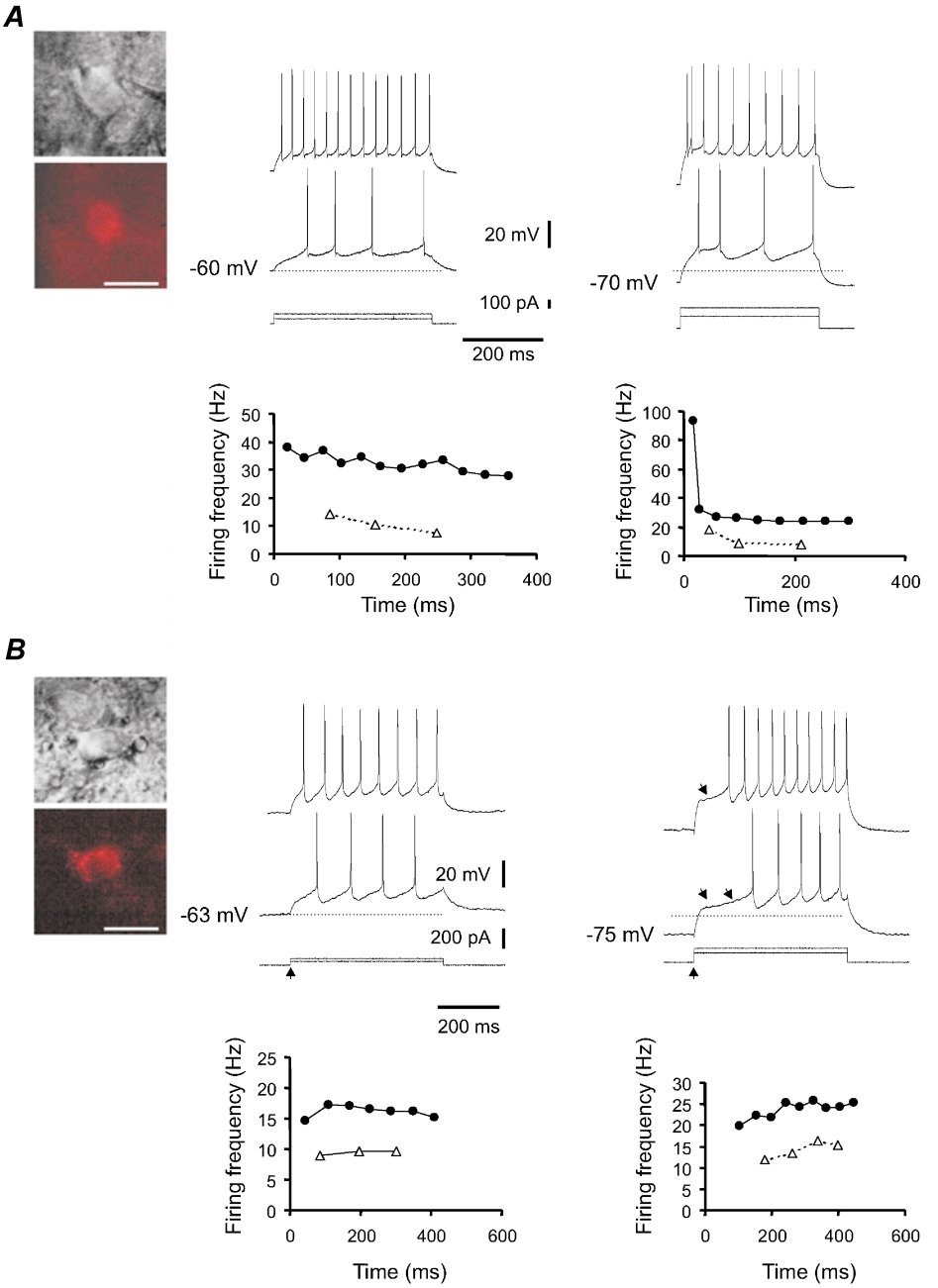

Figure 1. Firing pattern of BaMns and DaMns

A, firing behaviour of BaMns. Inset, infrared video-microscopic (top) and fluorescence (bottom) pictures of a retrogradely labelled BaMn (calibration bar, 25 μm). Firing properties of a P6 BaMn. Current pulses of various amplitude elicited trains of APs from the resting membrane potential (−60 mV, left panels) and from a hyperpolarized potential (−70 mV, right panels). In each experimental condition, the instantaneous firing frequency has been plotted *versus* the latency of each AP (△, smaller current pulses; ●, larger current pulses). Note that the frequency decreased over time in all cases but the drop of frequency was more marked when the neuron was held at −70 mV. *B*, firing behaviour of DaMns. Inset, infrared video-microscopic (top) and fluorescent (bottom) pictures of a retrogradely labelled DaMn (calibration bar, 25 μm). Firing properties of a P7 DaMn. Current pulses of variable amplitude elicited trains of APs from the resting membrane potential (−63 mV, left panels) and from a hyperpolarized potential (−75 mV, right panels). In each experimental condition, the instantaneous firing frequency has been plotted *versus* the latency of each AP (△, small current pulse; ●, larger current pulse). Note that the frequency slightly increased over time in all cases but that a delay in the firing (black arrows) was more prominent when the neuron was held at −75 mV.

mean index of accommodation was $r = 1.11 \pm 0.02$ ($n = 23$). They were observed between P4 and P9 (maximum near 50 % at P6–P7, Fig. 2*C* and *D*), but were never encountered before P4 (0/6 neurons) or after P9 (0/8 neurons), indicating a transient expression. In addition, they exhibited several immature characteristics: an action potential with a simple AHP (Fig. 3*B* and *C*), a linear current–voltage relationship and a large input resistance (591 ± 66 MΩ, $n = 23$). The input resistance of these neurons was significantly larger than that of BaMns at the same age ($P < 0.01$). The general characteristics of DaMns have been summarized in Table 1.

We conclude that aMns exhibit two complementary firing profiles: motoneurons exhibiting an initial burst firing and motoneurons with a delayed excitation. The first category corresponds to aMns encountered in adult rats *in vivo* (Durand, 1989). In the rest of the experiments, we characterized the currents that determine each type of firing.

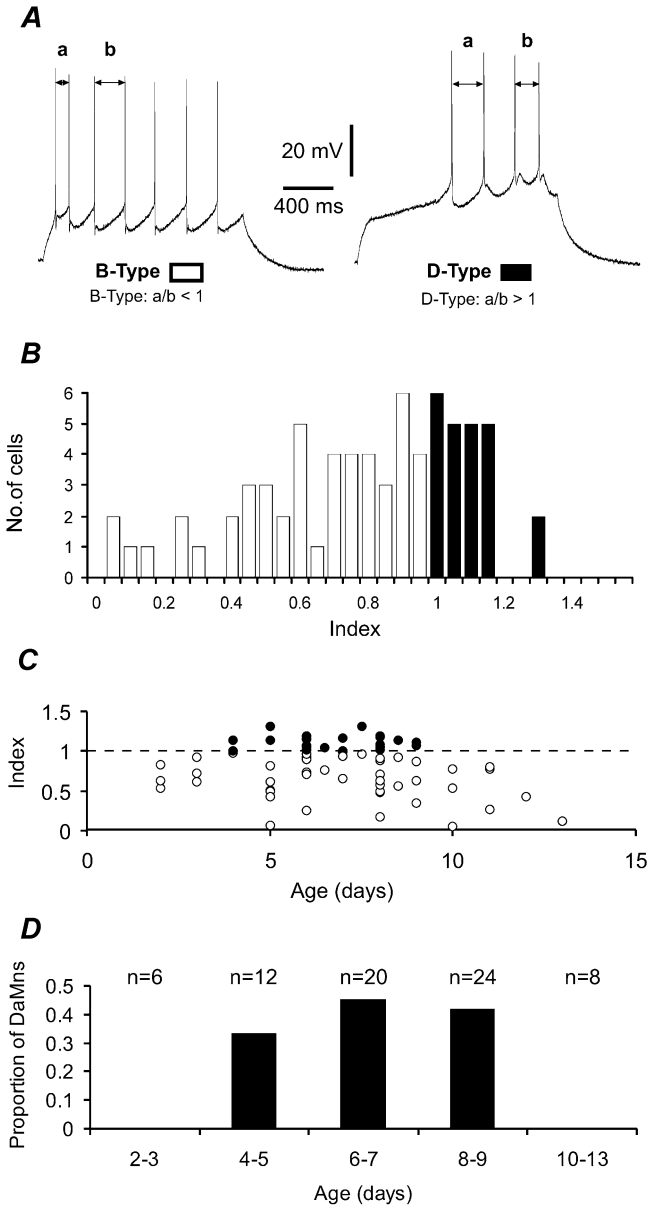

Figure 2. Classification and developmental profile of aMns

A, the index of firing accommodation was calculated as the ratio of the first interspike interval (*a*) to that of the third interspike interval (*b*). B-type aMns exhibited a ratio smaller than 1 whereas D-type aMns exhibited a ratio larger than 1. *B*, distribution of the index of accommodation (open bars BaMns, filled bars, DaMns). *C*, developmental profile of BaMns (○) and DaMns (●). *D*, proportion of DaMns in 5 classes of postnatal age. Note that no DaMns were encountered in 10- to 13-day-old rats.

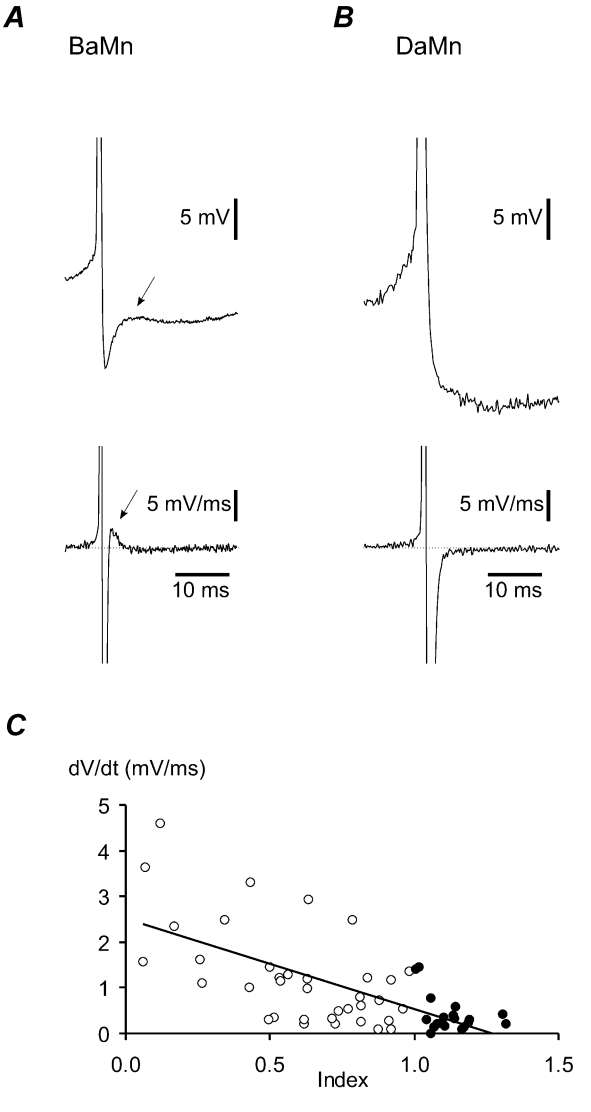

Figure 3. Action potential waveform of BaMns and DaMns

A and *B*, comparison of the afterhyperpolarization (AHP, upper traces) and its derivative (bottom traces) in BaMns and DaMns. Note the complex AHP in BaMns characterized by a fast AHP, an afterdepolarization (black arrow) and a medium AHP. *C*, the amplitude of the positive peak on the derivative (○, BaMns; ●, DaMns) was measured systematically in all aMns (dV/dt). The amplitude of this positive peak was inversely correlated with the index of accommodation ($y = -2x + 2.5$, $R = 0.66$; $n = 54$).

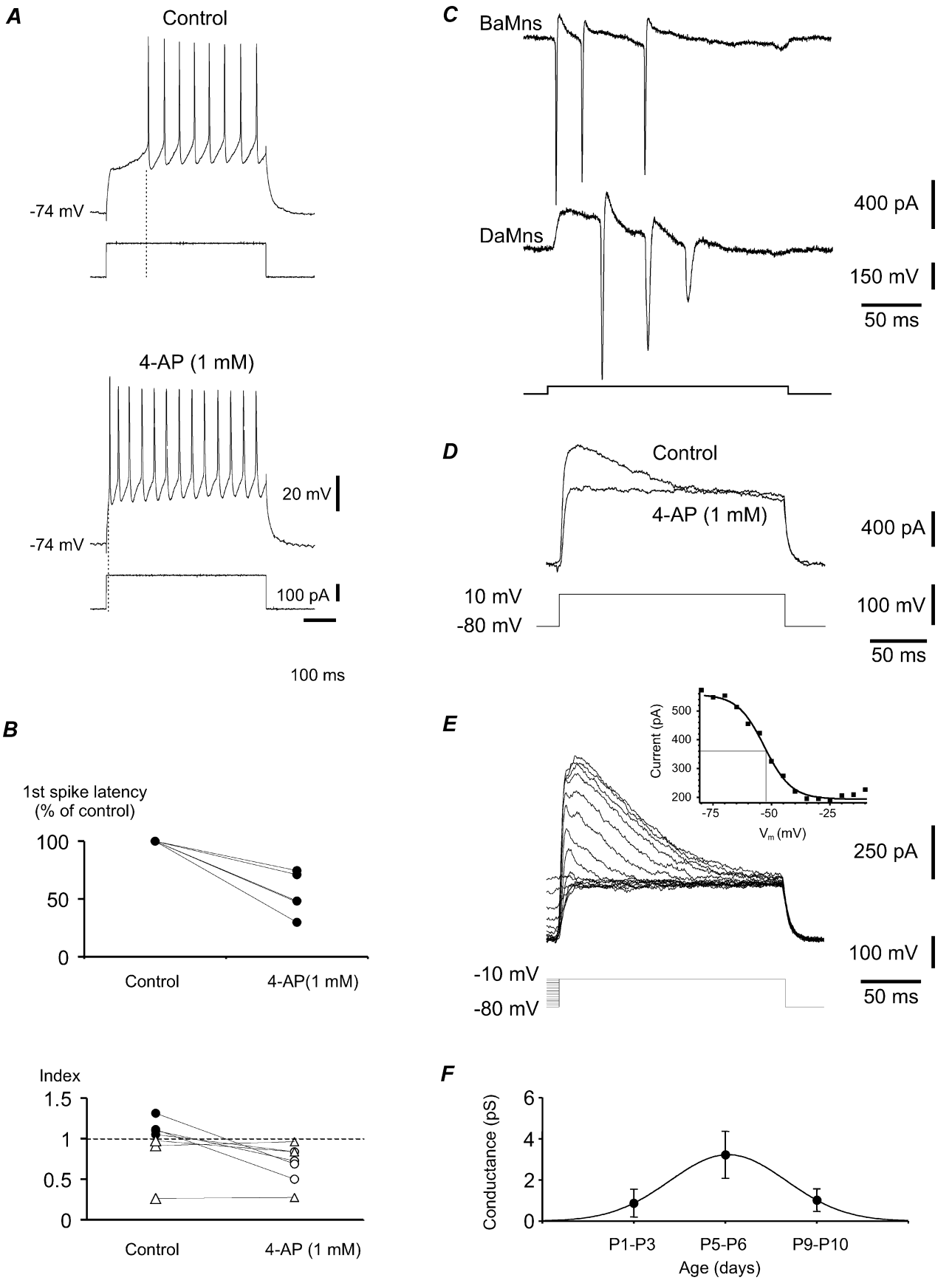

Figure 4. For legend see facing page.

A-type K^+ current determines the firing profile of DaMns

The delayed excitation that characterized DaMns was studied pharmacologically when the membrane potential of the neurons was held at a potential slightly more negative than −70 mV. Trains of APs were evoked in DaMns at a frequency of ~10 Hz. In the presence of 1 mM 4-amino-pyridine (4-AP), the latency of the first AP measured from the onset of the current pulse decreased to 54 ± 8 % (n = 5, Fig. 4*A* and *B*). These data indicate that a 4-AP-sensitive potassium current largely determines the firing properties of DaMns. In addition, the index of accommodation shifted towards lower values (from 1.142 ± 0.06 to 0.686 ± 0.07, n = 4, Fig. 4*B*). The same manipulation had, however, no significant effect on BaMns' firing behaviour (index from 0.717 ± 0.23 to 0.690 ± 0.21, n = 3, Fig. 4*B*), indicating that in contrast to DaMns, BaMns' firing profile is not principally determined by A-type potassium currents. Thus, we found that the presence of a prominent 4-AP-sensitive current is sufficient to functionally distinguish DaMns and BaMns.

Voltage-gated potassium currents were studied in DaMns recorded in voltage-clamp conditions. A large outward current that was able to delay the first action current was seen when a step depolarization was applied through the patch electrode in DaMns but not in BaMns (Fig. 4*C*). In the presence of the sodium channel blocker tetrodotoxin (TTX, 1 μM) and the calcium channels blockers, Ni^{2+} (200–400 μM) and cadmium (125 μM), step depolarizations from −80 mV to −10 mV evoked a transient outward current (decay time constant of 28.8 ± 6.2 ms at −10 mV, n = 4) followed by a sustained outward current (Fig. 4*D*). 4-AP (1 mM) blocked the transient component but not the non-inactivating component (n = 5 cells, Fig. 4*D*). The transient component was also found to be sensitive to the membrane potential. The transient current inactivated when the neuron was depolarized near the resting membrane potential (half inactivation at −52.3 ± 0.3 mV, n = 3 neurons, Fig. 4*E*). We conclude that DaMns display an inactivating outward current that is sensitive to 4-AP.

We next determined the developmental profile of the A-type current in aMns. At an early stage (P1–P3), the conductance of the transient outward current was 0.87 ± 0.67 nS (n = 3). It increased to 3.22 ± 1.14 nS (n = 5) at P5–P6 and declined to 1.02 ± 0.55 nS at P9–P10 (n = 4) (Fig. 4*F*). These data confirm the transient expression of DaMns during development.

In DaMns, the blockade of the 4-AP-sensitive outward current also modified the adaptation of the AHP during repetitive firing. In fact, the magnitude of the AHP progressively decreased over the train of spikes in control conditions. The amplitude of the fifth AHP was on average 67 ± 3 % of that of the first AHP (n = 4 cells; Fig. 5*A* and *B*). In the presence of 1 mM 4-AP, no decrement in the AHP was observed (the amplitude of the fifth AHP increased to 103 ± 2 % of that of the first AHP (n = 3 cells; Fig. 5*B* and *D*)).

As stated earlier, DaMns are characterized by a monophasic AHP following the first AP. However, examination of later spikes revealed that a significant fraction of these neurons expressed a complex AHP (9/23, see Fig. 5*A*) In the presence of 4-AP, the width of the AP became broader and the fast AHP was blocked (Fig. 5*A* and *C*). The mAHP amplitude increased as a result of the possible enhancement of the calcium influx associated with each AP. We conclude that in addition to delaying the firing and determining the progressive acceleration of the instantaneous firing frequency, the A-type K^+ current contributes to the AHP in DaMns.

Role of T-type Ca^{2+} current in the firing of BaMns

BaMns were characterized by an initial burst evoked by a depolarizing current pulse from a hyperpolarized resting potential (Figs 1*A* and 6*A*). A rebound burst was initiated when a transition of the membrane potential to a voltage near −60 mV was reached (threshold, −64 ± 1 mV, not

Figure 4. A-type K^+ currents shape the firing properties of DaMns

A, application of 4-AP (1 mM) blocked the delay of firing in a P7 DaMn and revealing a firing pattern typical of a BaMn. *B*, summary of the normalized change in the latency of the first spike (top panel) and in the accommodation index induced by 1 mM 4-AP (bottom panel) for BaMns (●) and DaMns (△). Note that all DaMns (index > 1) behaved as BaMns in the presence of 4-AP (index < 1) whereas the BaMns remained unchanged. *C*, complex currents generated by pulse depolarization from −80 mV to −30 mV in a BaMn (top panel) and DaMn (bottom panel). Note the presence of a fast outward current that precedes the generation of the first sodium inward current. *D*, block of the transient outward current by 4-AP in a DaMn. Outwards currents were recorded in the presence of 2 mM kynurenate, 100 μM picrotoxin, 1 μM strychnine, 1 μM TTX, 200 μM Ni^{2+}, 125 μM Cd^+. Bath application of 1 mM 4-AP blocked the transient component of the outward current. *E*, inactivation of the transient outward current. The outward current was evoked by a step from −80 mV to −10 mV. The amplitude of this current was reduced by half when a 200 ms depolarizing prepulse to near −55 mV was applied (see graph in the inset, inactivation curve fitted with a Boltzmann equation ($I = A_1 + A_2/(1 + \exp((V_m - V_{½})/k)$, k = −5.7, where A_1 is the minimal current value, A_2 is the maximal current value, V_m is the conditioning potential, $V_{½}$ is the half inactivation potential and k is the slope factor)). *F*, development of the I_A conductance in aMns.

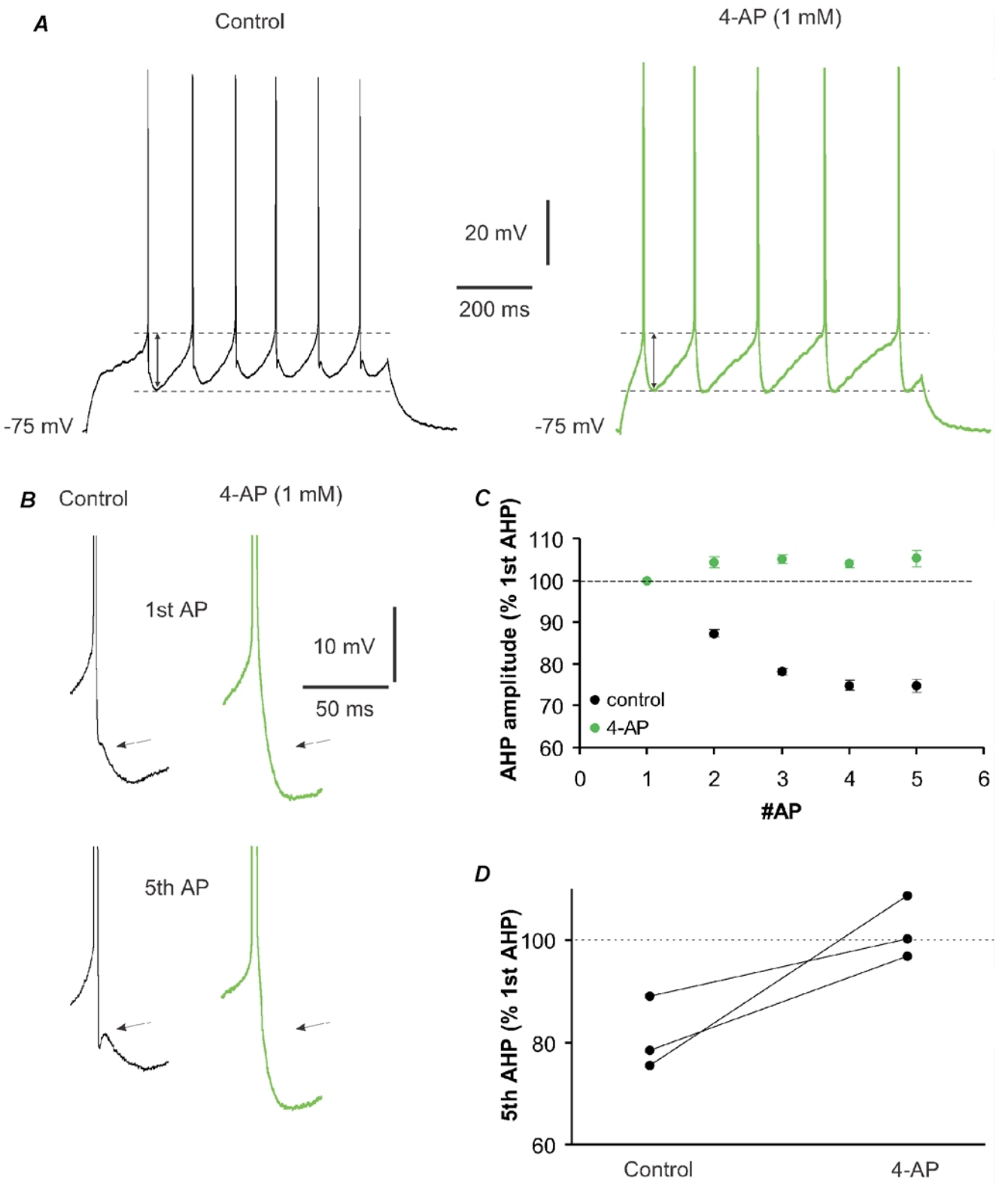

Figure 5. 4-AP-sensitive current shapes the AHP of DaMns

A, comparison of the AHP amplitude during repetitive firing in control conditions (left) and in the presence of 4-AP (right) in a P9 DaMn. Note the progressive decrease in the AHP amplitude in control conditions. *B*, enlargement of the first (top) and fifth AP (bottom) in control conditions and in the presence of 1 mM 4-AP. Note the blockade of the fast AHP component in the repolarizing phase of the APs. *C*, evolution of the AHP amplitude during discharge. The AHP was normalized to that of the first spike. An attenuation was observed in control conditions but not in the presence of 4-AP. *D*, pooled data showing the systematic blockade of the attenuation of the AHP amplitude ($n = 3$ cells).

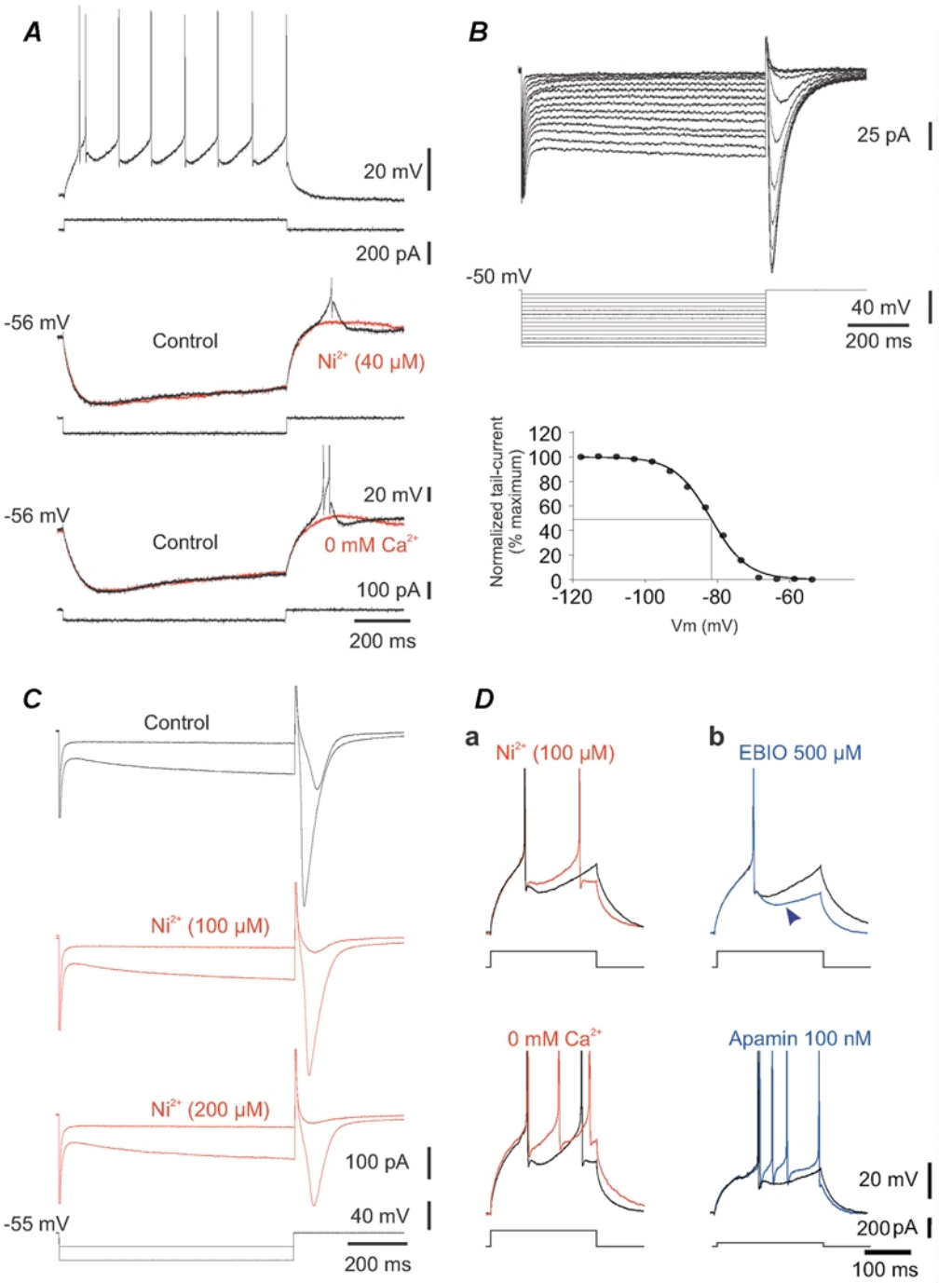

Figure 6. T-type Ca^{2+} current in BaMns

A, burst of APs in a BaMn recorded from a P13 rat. The inversion of the polarity of the current pulse evoked a slow rebound potential that elicited a fast action potential. The rebound potential was blocked by a low concentration of Ni^{2+} or by lowering the external concentration of Ca^{2+}. *B*, recovery from inactivation of the transient inward tail-current by a hyperpolarization in a BaMn (holding potential −50 mV). The patch pipette contained 140 mM Cs^{+} and recordings were made in the presence of 1 μM TTX. The increment of the voltage step evoked a transient inward current. Lower graph, normalized current amplitude *versus* voltage fitted with a Boltzmann equation ($(I = A_1 + A_2/(1 + \exp((V_m - V_{½})/k)$, $k = -5$). The half-current amplitude was obtained for a hyperpolarization of −82 mV. *C*, effect of low concentration of external Ni^{2+}. Two hyperpolarizing pulses were used. In the presence of nickel (100–200 μM), the inward current evoked by the small hyperpolarization was completely blocked and that evoked by a larger hyperpolarization was reduced by half. *D*, role of T-type Ca^{2+} current and the shaping of the AHP of BaMns. Black traces are controls. *Da*, reduction of the medium AHP by 100 μM Ni^{2+} (top) or by lowering the external concentration of Ca^{2+} (bottom). *Db*, bath application of the SK channel activator EBIO (500 μM) strongly enhanced the medium AHP (arrowhead, top). Apamin (100 nM) blocked the mAHP (bottom).

shown). The rebound potential was also evoked by a current-induced hyperpolarization when the neuron was held at a membrane potential between −55 and −60 mV (Fig. 6*A*). This rebound was observed in the majority of the BaMns tested (31/35) and was systematically observed after P7 (Table 2). In contrast, DaMns exhibiting a rebound potential in control conditions were encountered in only a few cases (1/23). This proportion is probably underestimated because of the antagonist action of the A-type current. In fact, a depolarizing rebound could be unmasked by 4-AP in DaMns exhibiting a complex AHP on the late APs ($n = 2$, not shown). These data suggest that a correct estimate of the presence of T-type current is close to one-third (i.e. the proportion of DaMns with a complex AHP on the late spike).

In voltage-clamp recordings with intracellular caesium and in the presence of TTX and TEA, a transient hyperpolarization from −50 to −70 mV evoked an inward tail current that progressively increased with the amplitude of the hyperpolarizing pulse (Fig. 6*B*). In these conditions, the half recovery from inactivation of the current occurred at −79 ± 4 mV ($n = 4$).

We next characterized this inward tail-current pharmacologically. The rebound potential was blocked by low concentrations of Ni^{2+} (10–40 μM) or by lowering the external calcium concentration to nominally 0 mM (Fig. 6*A*, $n = 7$). The inward current was also blocked by low concentrations of Ni^{2+} (100–200 μM) (Fig. 6*C*, $n = 4$) or by mibefradil (5–10 μM, 55 ± 15 % of the control amplitude, $n = 3$). We conclude that BaMns express a T-type calcium current.

Currents underlying the mAHP in BaMns

T-type Ca^{2+} current was found to determine the medium AHP of action potentials recorded in BaMns. In these experiments, a brief depolarizing current pulse was injected into BaMns in order to elicit a single action potential. In the presence of 40–100 μM Ni^{2+} the shape of

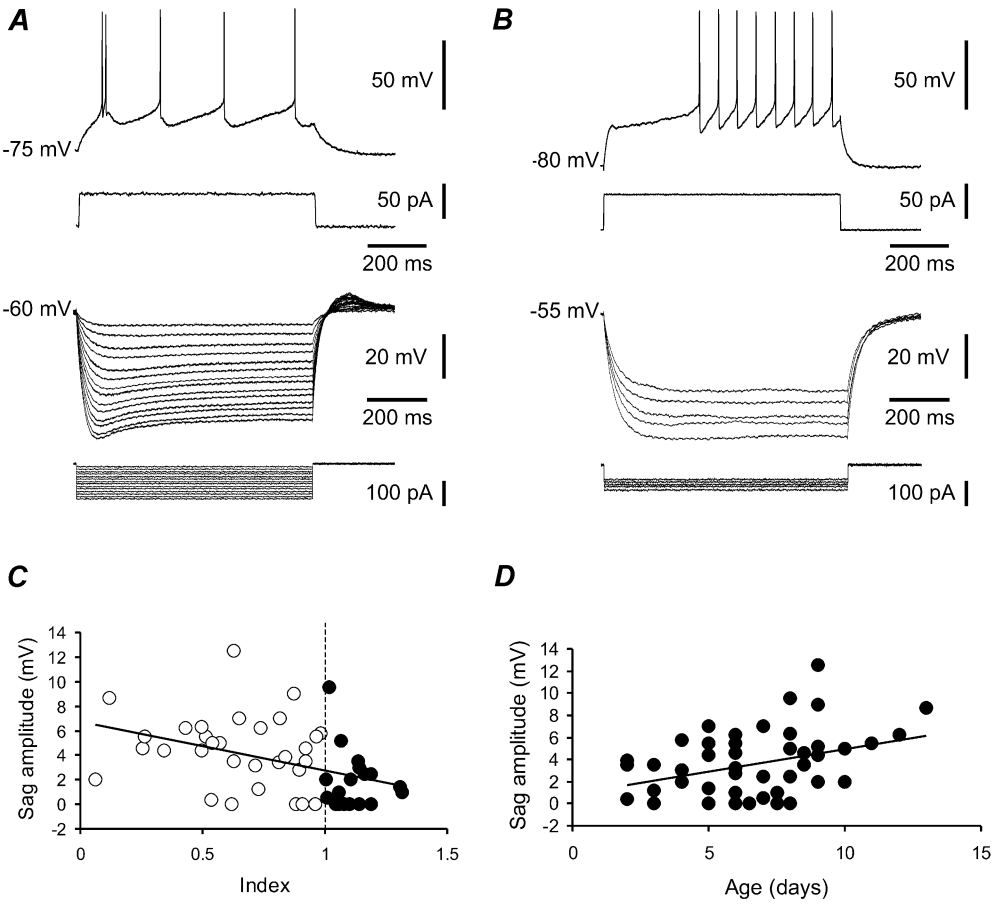

Figure 7. Depolarizing sag in BaMns but not in DaMns

A, voltage responses (upper traces) to positive and negative current steps (lower traces) injected via the recording pipette during whole-cell current-clamp recording of a BaMn. *B*, voltage responses (upper traces) to positive and negative current steps (lower traces) injected via the recording pipette during whole-cell current-clamp recording of a DaMn. No depolarizing sag was visible, even when large hyperpolarizations were induced. *C*, plot of the sag amplitude *versus* the index of firing accommodation (linear regression, $y = -4.0x + 6.48$, $R = 0.42$, $n = 47$). *D*, plot of the sag amplitude as a function of postnatal development (linear regression $y = 0.4x + 0.8$, $R = 0.35$, $n = 47$).

the AHP changed considerably. The most striking observation was a decrease in the amplitude of the mAHP (Fig. 6*Da*), as previously shown for other brainstem neurons (Viana *et al.* 1993*b*; Williams *et al.* 1997). Lowering the external concentration of calcium significantly reduced the amplitude of the mAHP (Fig. 6*Da*, $n = 3$ and 4 respectively).

The decrease of the mAHP amplitude by Ni^{2+} or by lowering the external calcium concentration indicates that the calcium influx mediated by T-type calcium channels might activate Ca^{2+}-dependent potassium currents. Because of the relatively fast time course of this mAHP, we investigated the role of small conductance Ca^{2+}-activated K^+ (SK) channels. We tested the effect of the SK channel activator 1-ethyl-2-benzimidazolinone (EBIO) (Pedarzani *et al.* 2001) on the mAHP elicited by a single action potential. The bath application of EBIO (500 μM) dramatically increased the amplitude of the medium AHP but did not affect the fAHP (Fig. 6*Db*, $n = 3$). Conversely, the SK channel blocker apamin (100 nM) blocked the mAHP (Fig. 6*Db*, $n = 3$). We conclude that T-type Ca^{2+} current expressed in BaMns determines the mAHP amplitude through the activation of SK channels.

H-type cationic conductance in BaMns

A depolarizing sag has been reported in rat aMns *in vivo* when the neurons were hyperpolarized by current pulses (Durand, 1989). We therefore investigated whether this sag was also present in developing aMns *in vitro*.

BaMs responded to hyperpolarizing current pulses (from a holding potential of −55 to −65 mV; $n = 16$) with a slow depolarizing sag back to the holding potential (Fig. 7*A*). The amplitude of this sag (calculated by subtracting the steady-state potential measured just before the offset of negative current steps from the peak potential) increased with the magnitude of peak voltage deflections. In contrast, DaMns exhibited no depolarizing rectification, even when the amplitude of the hyperpolarization exceeded −50 mV (Fig. 7*B*). The sag amplitude evoked by a hyperpolarization of −30 mV from the resting membrane potential was found to be negatively correlated with the index of accommodation of the neurons (Fig. 7*C*). These observations indicate that the I_H current is almost exclusively expressed in BaMns.

We next studied the influence of age on the expression of the H-current in aMns. The amplitude of the depolarizing sag evoked by hyperpolarizations of −30 mV was

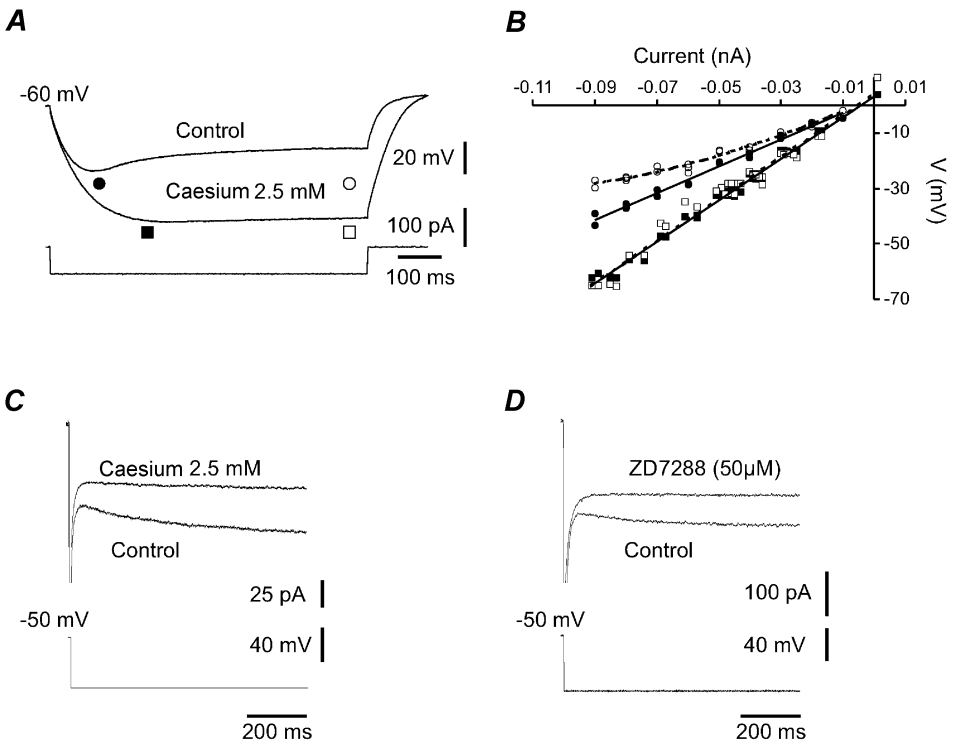

Figure 8. Pharmacology of H-current in BaMns

A, voltage response to a negative current step in the absence (control) and in the presence of 2.5 mM caesium after compensation of the hyperpolarization by constant positive current. Note the large increase in the input resistance of the neuron. Voltage deflections were measured at the first peak of hyperpolarization (● and ■) and just before the offset of the negative current step (○ and □). *B*, voltage deflections *versus* amplitude of the negative current pulse before (● and ○) and after application of 2.5 mM Cs^+ (■ and □). *C* and *D*, current responses recorded under whole-cell voltage-clamp (holding potential −50 mV) evoked by hyperpolarizing voltage step in control and in the presence of 2.5 mM Cs^+ (*C*) or 50 μM ZD7288 (*D*).

positively correlated with age. In particular, a significant depolarizing sag was systematically observed in aMns recorded from rats older than 9 days (Fig. 7*D*). These data indicate a developmental increase in the percentage of aMns expressing the H-current, as reported in hypoglossal (Bayliss *et al.* 1994) and ocular motoneurons (Tsuzuki *et al.* 1995).

The application of 2.5 mM external caesium abolished the depolarizing sag during negative current steps and led to a substantial membrane hyperpolarization (−6.2 ± 0.9 mV, $n = 6$ neurons) and an increase in the input resistance (from 485 ± 66 MΩ to 887 ± 166 MΩ, $n = 6$, Fig. 8*A* and *B*). The input resistance in the presence of H-current blockers was virtually identical to that observed in DaMns, suggesting that the difference in input resistance observed between DaMns and BaMns might simply result from a differential expression of the I_H current. This point is further supported by the negative correlation observed between the amplitude of the sag evoked by a hyperpolarization of −30 mV and the input resistance of the neuron (input resistance *vs.* sag, linear regression $y = -41x + 600$, $R = 0.46$, $n = 47$ neurons not shown). To further explore the properties of this current we made somatic whole-cell voltage-clamp recordings in the presence of TTX. Under these conditions, negative voltage steps delivered from a holding potential of −50 mV activated slow inward currents, which were abolished by the application of external caesium (Fig. 8*C*). In other neurons, the bath application of the selective and irreversible pharmacological blocker of I_H, ZD7288 (Bosmith *et al.* 1993; Harris & Constanti, 1995), blocked the slow inward current (Fig. 8*D*; $n = 8$). We conclude that B-type aMns display the I_H current.

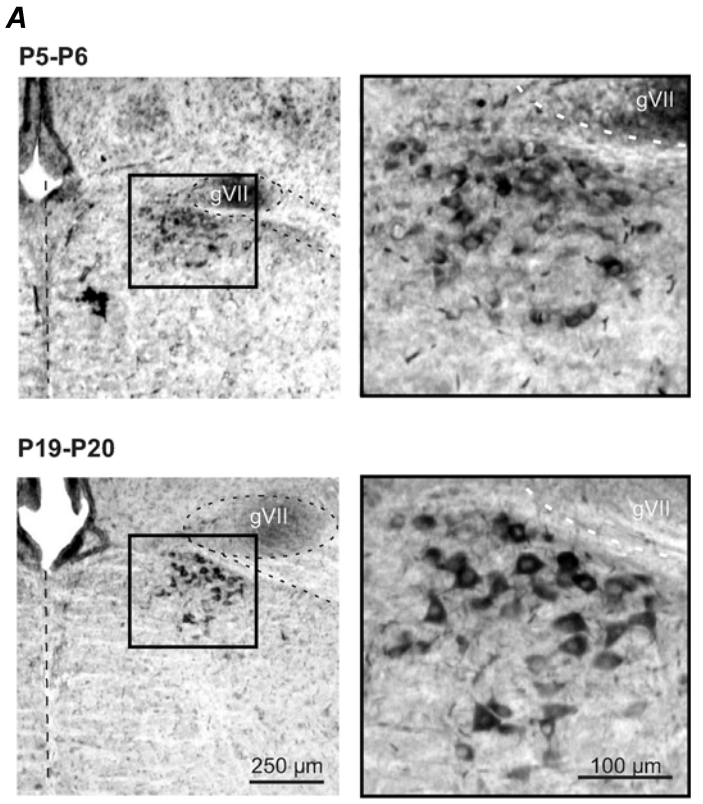

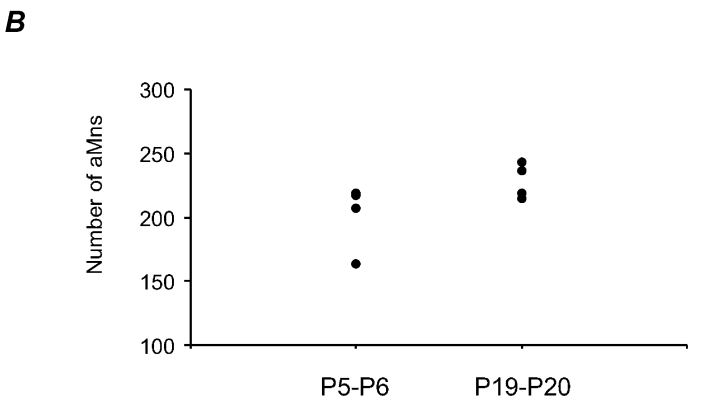

Figure 9. Stability of the number of aMns during development

A, immunohistochemical labelling of ChAT in the brainstem of a P5–P6 rat (upper panels) and in a P19–P20 rat (lower panels). Left, the midline is symbolized by a dashed vertical line. Right, magnification of the abducens nucleus. The area of the genu of the nerve VII (gVII) is delimited by dashed perimeters. *B*, quantification of aMns in P5–P6 and P19–P20 rats ($n = 4$ nuclei in each case).

Stability of the number of aMns during postnatal development

Our data indicate that two types of aMn coexist during a brief period of development and only BaMns remain at the adult stage. Thus, two alternative developmental hypotheses can be considered. First, DaMns may evolve in the BaMns type during development as a result of a process of instruction in which the expression of intrinsic currents may be regulated. Alternatively, the selection hypothesis would propose that only the adult motoneuron type is selected during the developmental process. If this second hypothesis were correct, the number of aMns should be significantly higher when both types are present. We therefore performed immunohistochemical labelling of ChAT to determine the number of aMns at P5–P6 and at P19. No significant changes in the number of aMns was found at each developmental stages (202 ± 13 ChAT-positive aMns at P5–P6, $n = 4$ abducens nuclei and 228 ± 7 ChAT-positive aMns at P19–P20, $n = 4$ abducens nuclei, Fig. 9*A* and *B*, $P > 0.1$). We conclude that the D-type may correspond to a transient phenotype of developing aMns.

DISCUSSION

This study provides the first characterization of the electrophysiological properties of rat aMns *in vitro* during the first 2 weeks of postnatal development. Our data indicate that the acquisition of adult-like functional properties of aMns occurs near P10. Earlier, a significant fraction of aMns display immature properties. In addition to this developmental study, our data describe the main functional features of aMns. Identification of the voltage-gated currents underlying the intrinsic properties of rat aMns is a pre-requisite for later modelling and physiological studies.

Heterogeneous discharge profiles of developing aMns

We report here that aMns recorded in P2–P13 rats display a large variability in their discharge mode. In response to depolarizing current pulses, most of the motoneurons (BaMns) showed a firing profile with an initial burst followed by an accommodation of the instantaneous firing frequency. These neurons were characterized by the presence of a prominent T-type Ca^{2+} and H-type cationic current. Their firing behaviour resembled that reported in adult rat and cat abducens motoneurons *in vivo* (Baker & Highstein, 1975; Grantyn & Grantyn, 1978; Durand, 1989; Gonzales-Forero *et al.* 2002). The T-type Ca^{2+} current is responsible for the rebound potential activated by an hyperpolarization. This rebound potential was found to be blocked by low concentration of Ni^{2+} (10–40 μM) or by reducing the external concentration of Ca^{2+}. The underlying current was also blocked by mibefradil. The T-type calcium current was also found to determine the mAHP (slow component of the complex AHP) through the activation of calcium-dependent K^+ currents. Indeed, the blockade of the calcium influx or application of apamin decreased the mAHP whereas the SK channel activator EBIO increased the mAHP amplitude. It is interesting to note that mRNAs coding for the SK1 and SK2 subunits are highly expressed in aMns (Stocker & Pedarzani, 2000). The I_H is responsible for the relatively lower input resistance found in BaMns. Indeed the application of caesium increased the membrane resistance of BaMns to a value corresponding to that of DaMns.

A small fraction of neurons (DaMns) exhibited a delayed excitation and a progressive acceleration in instantaneous firing frequency. These neurons were found only from P4 to P9. The delayed excitation in DaMns was due to a 4-AP-sensitive outward current. This current inactivated near resting membrane potential and had a decay time constant close to 30 ms. These properties are similar to the A-type K^+ current reported in spinal (Takahashi, 1990) and hypoglossal motoneurons (Lape & Nistri, 1999). In addition to a shorter spike latency, blockade of I_A also increased the mAHP amplitude. This may result from broadening of the AP that enhanced the calcium influx associated with each AP. DaMns were encountered only between P4 and P9 and displayed several characteristics of immature neurons. Their first action potential displayed a simple AHP and these neurons had a high input resistance that can be attributed to the lack of the H-type current. Indeed, the amplitude of the depolarizing sag activated by the hyperpolarization was negatively correlated with the index of firing accommodation.

The abducens nucleus of the rat contains separate populations of neurons: abducens motoneurons that innervate the lateral rectus muscle and internuclear neurons that project to the third oculomotor nucleus and correspond to 30 % of the neurons in the adult abducens nucleus (Labandeira Garcia *et al.* 1983; Cabrera *et al.* 1988). It appears however unlikely that DaMns correspond to internuclear neurons. Both DaMns and BaMns were located within the abducens nucleus and were retrogradely labelled by DiI (Fig. 1*A* and *B*). In addition, neurons with characteristics of typical aMns were selected for patch-clamp recordings, i.e. with a large soma (> 20 μm) with a ventro-medial position relative to the genu of the VIIth nerve (Cabrera *et al.* 1988). Finally, *in vivo* recordings during horizontal saccades suggest that interneurons and motoneurons display a phaso-tonic firing mode in the adult (Baker & Highstein, 1975; Delgado-Garcia *et al.*1986*a*,*b*). Thus, internuclear neurons might have been sampled in the population of BaMns but not in that of DaMns. However, one cannot totally exclude the possibility that interneurons also display a delayed firing during development. Although we cannot completely rule out the possible sampling of a small percentage of internuclear neurons in our study, the DaMn population

cannot solely correspond to the population of internuclear neurons. We therefore conclude that the neurons recorded in our study correspond to aMns.

Heterogeneous firing behaviour has been reported in other brainstem nuclei including developing hypoglossal motoneurons (Viana *et al.* 1995), developing facial motoneurons (Magariños-Ascone *et al.* 1999), neurons from the lateral superior olive (Adam *et al.* 1999), nucleus tractus solitarius neurons (Bailey *et al.* 2002) and medial vestibular nuclei in the adult rodent (Serafin *et al.* 1991). It is interesting to note that the developmental profile of hypoglossal motoneurons, that originate in a well characterized brainstem nucleus, is similar to that of aMns reported here. While most hypoglossal motoneurons recorded from young rats (< P4) are of type B, the majority of hypoglossal motoneurons recorded during the second postnatal week are of type D (Viana *et al.* 1995). At later developmental stages (> P21), firing reverts to a decrementing pattern (Viana *et al.* 1995). Thus, the transient expression of motoneurons with a delayed firing pattern appears to be a common property of brainstem motoneurons. This heterogeneity in a neuronal population is not transient in all brainstem nuclei. In adult vestibular neurons, two types of neurons can be differentiated on the basis of distinct expression of T-type Ca^{2+} and A-type K^+ currents but they may also form a continuous population (Serafin *et al.* 1991; du Lac & Lisberger, 1995). We conclude that functional heterogeneity within a well-defined nucleus may be a widespread property in brainstem neurons.

Do DaMns maturate into BaMns during postnatal development?

The functional dichotomy between BaMns and DaMns was not absolute since we observed a continuum between two extreme cases. In fact, the two functional indices we used to characterize the firing behaviour in terms of the index of firing adaptation or the derivative of the ADP exhibited a continuous distribution. In addition, several features of one type were also found in the other type, but to a lesser extent. First, the A-type potassium current that characterizes DaMns is also responsible for the fast AHP in BaMns. In addition, pharmacological blockade of the prominent early hyperpolarization by 4-AP transformed the typical D-type aMns into B-type aMns. T-type calcium current that is involved in generating the complex AHP in BaMns is also observed in a significant fraction of DaMns (see for instance Figs 2 and 5). Finally, the blockade of I_H in BaMns increased input resistance to values virtually identical to those observed in DaMns.

Our study indicates that BaMns neurons coexist with DaMns between P4 and P9. After P9, only BaMns were encountered. The number of ChAT-positive aMns remained constant at P5–P6 and at P19–P20. The numbers are similar to those reported previously for adult rat abducens nucleus (Cabrera *et al.* 1988). A simple explanation may be that the firing properties of aMns mature during development, allowing DaMns to evolve into BaMns. Taken together with the functional continuum, this constant number of aMns suggests a differential gradient of development of A-type K^+ current on the one hand and T- and H-type currents on the other hand. In hypoglossal motoneurons and oculomotor neurons, the hyperpolarization-activated cationic current displays a developmental expression profile that culminates at the adult stage (Bayliss *et al.* 1994; Viana *et al.* 1994; Tsuzuki *et al.* 1995; Cameron *et al.* 2000). The mRNAs encoding for I_H -channels (HCN1 and HCN2) are highly expressed in adult rat brainstem motoneurons (Santoro *et al.* 2000).

The developmental profile of other conductances is less straightforward. The 4-AP-sensitive A-type K^+ current that delays firing and shortens the AP becomes more prominent with age in nucleus tractus solitarius neurons (Vincent & Tell, 1997) but declines in developing phrenic motoneurons (Martin-Caraballo & Greer, 2000). It is thus possible that in aMns, both up- and down-regulation occurs. In fact, the number of DaMns with a prominent A-type current increased from P2–P3 to P4–P5, then the proportion of these neurons declined near P9–P10. This developmental profile is paralleled by the development of the A-type conductance: the mean conductance was low at P1–P3 and at P9–P10 but was maximal at P5–P6. The molecular substrate underlying this regulation will require further studies. The developmental profile of T-type current in motoneurons is also rather complex. Transient expression of the T-type Ca^{2+} current has been reported in brainstem and spinal motoneurons (Mynlieff & Beam, 1992; Viana *et al.* 1994; Martin-Caraballo & Greer, 1999; Plant *et al.* 1998). In spinal cord motoneurons, low-voltage-activated calcium channels become undetectable after P7–P8 (Mynlieff & Beam, 1992). In contrast, T-type current does not completely disappear in brainstem motoneurons. The rebound potential mediated by T-type calcium channels is always observed after P7 and can be recorded until P13 in aMns (see Fig. 6*A*). In addition, at the adult stage, the level of α1G and α1H mRNAs, two transcripts of the T-type calcium channel family is higher in brainstem motoneurons than in spinal motoneurons (Talley *et al.* 1999). Thus, it is conceivable that the T-type current is maintained in brainstem motoneurons.

The decline in T-type current observed in spinal motoneurons coincides with the phase of motoneuronal cell death (Mynlieff & Beam, 1992; Friedland *et al.* 1995; Perrier & Hounsgaard, 2000). This view is however not supported in the case of brainstem motor nuclei including the abducens nucleus since T-type calcium current could be clearly identified up to P13, long after the cell-death in brainstem motoneurons (from E16 to birth, Friedland *et*

al. 1995). Another possibility is that the maximum expression of T-type current corresponds to the establishment of motor function. In phrenic motoneurons, the expression of T-current is maximal just before birth (Martin-Caraballo & Greer, 1999)). Thus, it is possible that the large T-type current we observed during the second postnatal week is almost maximal at the time of eye opening (P11–P12). Later, this current might decline. Further study will be required to define more precisely the developmental gradient of the T-type current in aMns.

One of the conclusions of this study is that DaMns may mature into BaMns. Several studies have reported that synaptic or network activity induces rapid and long-lasting modifications in the firing behaviour of developing neurons (Desai *et al.* 1999; Aizenman & Linden, 2000). It is therefore possible that synaptic and circuit activity lead to the maturation of intrinsic neuronal properties of aMns by regulation of ionic conductances.

Does BaMn correspond to the adult aMn type?

DaMns were never encountered in rats older than P9 and BaMns were recorded only between P9 and P13. This upper limit was mainly dictated by technical reasons. Patch-clamp recording from well-identified motoneurons in this nucleus becomes very difficult in rats older than P8 because visibility within the nucleus abducens is strongly reduced by the abundant myelin from the VIIth nerve. Thus, we were not able to successfully record from aMns in rats older than P13. However, several lines of evidence indicate that the description of the firing properties we observed from P10 to P13 reflects the electrical properties of aMns in the adult rat reported *in vivo*. First, as in adult rat and cat aMns (Baker & Highstein, 1975; Grantyn & Grantyn, 1978; Durand, 1989; González-Forero *et al.* 2002), BaMns *in vitro* exhibited an action potential with a complex AHP. Similar to aMns from the adult rat (Durand, 1989), BaMns displayed an initial burst and adaptation of firing. Moreover, in agreement with previous *in vivo* studies (Durand, 1989), a depolarizing sag was observed in BaMns when hyperpolarizing pulses of current were injected into the neuron. Although these characteristics have not been extensively quantified in the adult rat *in vivo*, we conclude that BaMns display firing properties that resemble those described in the adult. Moreover, our data suggest that the functional properties of rat aMns reach maturity just before eye opening (P11–P12).

What are the functional properties that can be inferred from the voltage-gated currents determined in aMns? First, the phaso-tonic behavior of BaMns might be particularly relevant to compensate the inertia of the ocular globe (Baker & Highstein, 1975; Robinson, 1981). More interestingly, these neurons co-express T-type Ca^{2+} and H-type cationic currents which may participate in shaping of excitatory and inhibitory postsynaptic potentials (Reyes, 2001) and in entraining intrinsic oscillations (Bal & McCormick, 1997). Thus, it is possible that these currents participate in maintaining coherent oscillatory behaviour during slow frequency nystagmus, but also in ensuring stability of neuronal discharge (Gomez *et al.* 1986; Gonzalez-Forero *et al.* 2002).

REFERENCES

Adam TJ, Schwarz DWE & Finlayson PG (1999). Firing properties of chopper and delay neurons in the lateral superior olive of the rat. *Exp Brain Res* **124**, 489–502.

Aizenman C & Linden DJ (2000). Rapid, synaptically driven increases in the intrinsic excitability of cerebellar deep nuclear neurons. *Nat Neurosci* **3**, 109–111.

Bailey TW, Jin YH, Doyle MW & Andresen MC (2002). Vaniloid-sensitive afferents activate neurons with prominent A-type potassium currents in nucleus tractus solitarius. *J Neurosci* **22**, 8230–8237.

Baker R & Highstein SM (1975). Physiological identification of interneurons and motoneurons in the abducens nucleus. *Brain Res* **91**, 292–298.

Bal T & McCormick D (1997). Synchronized oscillations in the inferior olive are controlled by the hyperpolarization-activated cation current I_h. *J Neurophysiol* **77**, 3145–3156.

Bayliss DA, Viana F, Bellingham MC & Berger AJ (1994). Characteristics and postnatal development of a hyperpolarization-activated inward current in rat hypoglossal motoneurons *in vitro*. *J Neurophysiol* **71**, 119–128.

Bosmith RE, Briggs I & Sturgess NC (1993). Inhibitory actions of ZENECA ZD7288 on whole-cell hyperpolarization activated inward current (I_f) in guinea-pig dissociated sinoatrial node cells. *Br J Pharmacol* **110**, 343–349.

Cabrera B, Portillo F, Pasaro R & Delgado-Garcia JM (1988). Location of motoneurons and internuclear neurons within the rat abducens nucleus by means of horseradish peroxidase and fluorescent double labeling. *Neurosci Lett* **87**, 1–6.

Cameron WE, Nunez-Abades PA, Kerman IA & Hodgson TM (2000). Role of potassium conductances in determining input resistance of developing brain stem motoneurons. *J Neurophysiol* **84**, 2330–2339.

Delgado-Garcia JM, del Pozo F & Baker R (1986*a*). Behavior of neurons in the abducens nucleus of the alert cat. I. Motoneurons. *Neuroscience* **17**, 929–952.

Delgado-Garcia JM, del Pozo F & Baker R (1986*b*). Behavior of neurons in the abducens nucleus of the alert cat. II. Internuclear neurons. *Neuroscience* **17**, 953–973.

Desai NS, Rutherford LC & Turrigiano GG (1999). Plasticity in the intrinsic excitability of cortical pyramidal neurons. *Nat Neurosci* **2**, 515–520.

du Lac S & Lisberger SG (1995). Membrane and firing properties of avian medial vestibular nucleus neurons *in vitro*. *J Comp Physiol* **176**, 641–651.

Durand J (1989). Electrophysiological and morphological properties of rat abducens motoneurones. *Exp Brain Res* **76**, 141–152.

Friedland DR, Eden AR & Laitman JT (1995). Naturally occurring motoneuron cell death in rat upper respiratory tract motor nuclei: a histological, fast DiI and immunohistochemical study in the hypoglossal nucleus. *J Neurobiol* **27**, 520–534.

Godaux E & Chéron G (1993). Testing the common neural integrator hypothesis at the level of the individual abducens motoneurones in the alert cat. *J Physiol* **469**, 549–570.

Gómez C, Canals J, Torres B & Delgado-Garcia JM (1986). Analysis of the fluctuations of the interspike intervals of the abducens nucleus neurons during ocular fixation in the alert cat. *Brain Res* **381**, 401–404.

Gonzalez-Forero D, Alvarez FJ, de la Cruz RR, Delgado-Garcia JM & Pastor AM (2002). Influence of afferent synaptic innervation on the discharge variability of cat abducens motoneurones. *J Physiol* **541**, 283–299.

Grantyn R & Grantyn A (1978). Morphological and electrophysiological properties of cat abducens motoneurones. *Exp Brain Res* **31**, 249–274.

Harris NC & Constanti A (1995). Mechanisms of block by ZD7288 of the hyperpolarization-activated inward rectifying current in guinea pig substantia nigra neurons *in vitro*. *J Neurophysiol* **74**, 2366–2378.

Labandeira Garcia JL, Gomez-Segade LA & Suarz Nunez JM (1983). Localisation of motoneurons supplying the extra-ocular muscles of the rat using horseradish peroxidase and fluorescent double labeling. *J Anat* **137**, 247–261.

Lape R & Nistri A (1999). Voltage-activated K^+ currents of hypoglossal motoneurons in a brain stem slice preparation from the neonatal rat. *J Neurophysiol* **81**, 140–148.

Magariños-Ascone C, Nunez A & Delgado-Garcia JM (1999). Different discharge properties of rat fascial nucleus motoneurons. *Neuroscience* **94**, 879–886.

Martin-Caraballo M & Greer JJ (1999). Electrophysiological properties of rat phrenic motoneurons during perinatal development. *J Neurophysiol* **81**, 1365–1378.

Martin-Caraballo M & Greer JJ (2000). Development of potassium conductances in perinatal rat phrenic motoneurons. *J Neurophysiol* **83**, 3497–3508.

Murphy GJ & du Lac S (2001). Postnatal development of spike generation in rat medial vestibular nucleus neurons. *J Neurophysiol* **85**, 1899–1906.

Mynlieff M & Beam KG (1992). Developmental expression of voltage-dependent calcium currents in identified mouse motoneurons. *Dev Biol* **152**, 407–410.

Pedarzani P, Mosbacher J, Rivard A, Cingolani LA, Oliver D, Stocker M, Adelman JP & Fakler B (2001). Control of electrical activity in central neurons by modulating the gating of small conductance Ca^{2+}-activated K^+ -channels. *J Biol Chem* **276**, 9762–9769.

Perrier J-F & Hounsgaard J (2000). Development and regulation of response properties in spinal motoneurons. *Brain Res Bull* **53**, 529–535.

Plant TD, Schirra C, Katz E, Uchitel OD & Konnerth A (1998). Single-cell RT-PCR and functional characterization of Ca^{2+} channels in motoneurons of the rat facial nucleus. *J Neurosci* 18, 9573–9574

Rekling JC, Funk GD, Bayliss DA, Dong XW & Feldman JL (2000). Synaptic control of motoneuronal excitability. *Physiol Rev* **80**, 767–852.

Reyes A (2001). Influence of dendritic conductances on the input-output properties of neurons. *Annu Rev Neurosci* **24**, 653–675.

Robinson DA (1981). Control of eye movements. In *Handbook of Physiology*, pp. 1275–1320. Williams and Wilkins, Bethesda.

Russier M, Kopysova IL, Ankri N, Ferrand N & Debanne D (2002). GABA and glycine co-release optimizes functional inhibition in rat brainstem motoneurons *in vitro*. *J Physiol* **541**, 123–137.

Santoro B, Chen S, Lüthi A, Pavlidis P, Shumyatsky GP, Tibbs GR & Siegelbaum SA (2000). Molecular and functional heterogeneity of hyperpolarization-activated pacemaker channels in the mouse CNS. *J Neurosci* **20**, 5264–5275.

Serafin M, de Waele C, Khateb A, Vidal PP & Mühlethaler M (1991). Medial vestibular nucleus in the guinea-pig. *Exp Brain Res* **84**, 417–425.

Stocker M & Pedarzani P (2000). Differential distribution of three Ca^{2+}-activated K^+ channel subuntits, SK1, SK2, and SK3 in the adult rat central nervous system. *Mol Cell Neurosci* **15**, 476–493.

Storm JF (1987). Intracellular injection of a Ca^{2+} chelator inhibits spike repolarization in hippocampal neurons. *Brain Res* **435**, 387–392.

Storm JF (1990). Potassium currents in hippocampal pyramidal cells. *Prog Brain Res* **83**, 161–187.

Takahashi T (1990). Membrane currents in visually identified motoneurons of neonatal rat spinal cord. *J Physiol* **423**, 27–46.

Talley EM, Cribbs LL, Lee JH, Daud A, Perez-Reyes E & Bayliss DA (1999). Differential distribution of a gene-family encoding low voltage-activated (T-type) calcium channels. *J Neurosci* **19**, 1895–1911.

Tsuzuki S, Yoshida S, Yamamoto T & Oka H (1995). Developmental changes in the electrophysiological properties of neonatal rat oculomotor neurons studied *in vitro*. *Neurosci Res* **23**, 389–397.

Viana F, Bayliss DA & Berger AJ (1993*a*). Calcium conductances and their role in the firing behavior of neonatal rat hypoglossal motoneurons. *J Neurophysiol* **69**, 2137–2149.

Viana F, Bayliss DA & Berger AJ (1993*b*). Multiple potassium conductances and their role in action potential repolarization and repetitive firing behavior of neonatal rat hypoglossal motoneurons. *J Neurophysiol* **69**, 2150–2163.

Viana F, Bayliss DA & Berger AJ (1994). Postnatal changes in rat hypoglossal motoneuron membrane properties. *Neuroscience* **59**, 131–148.

Viana F, Bayliss DA & Berger AJ (1995). Repetitive firing properties of developing rat brainstem motoneurones. *J Physiol* **486**, 745–761.

Vincent A & Tell F (1997). Postnatal changes in electrophysiological properties of rat nucleus tractus solitarii neurons. *Eur J Neurosci* **9**, 1612–1624.

Umemiya M & Berger AJ (1994). Properties and function of low- and high-voltage-activated Ca^{2+} channels in hypoglossal motoneurons. *J Neurosci* **14**, 5652–5660.

Williams S, Serafin M, Mühlethaler M & Bernheim L (1997). Distinct contributions of high- and low-voltage-activated calcium currents to afterhyperpolarizations in cholinergic nucleus basalis neurons of the guinea pig. *J Neurosci* **17**, 7307–7315.

Acknowledgements

We thank Drs J. M. Delgado-Garcia and P. P. Vidal for stimulating discussions, Drs U. Gerber and O. Caillard for helpful comments on the manuscript and Dr M. Seagar for his support. We thank Drs J. Nargeot and P. Lory (CNRS Montpellier) for the kind gift of Mibefradil. This work was supported by the Roche Research Foundation (to M. R.), Fondation pour la Recherche Médicale, Ministère de la Recherche et de la Technologie (ACI 'Jeunes Chercheurs') and Institut National de la Santé et de la Recherche Médicale (INSERM, programme 'Avenir').